Analysis of Thermal Radiation Bidirectionally Reflected from Roughened Brass

D. C. Look*
University of Missouri at Rolla, Rolla, Mo.

Thermal radiant power (energy/time) reflected from a series of carefully prepared, roughened, brass surfaces has been investigated experimentally. The data were acquired by holding the angle of incidence constant and varying the angle of reflection. A four parameter empirical equation fits the data to within 10% for a very wide range of laboratory variables. These variables include variations in the incidence angle of from 10° to 80° and in the reflected angle from 8° to 90°. Surface roughnesses can be described as ranging from "mirror-like" to nearly "diffuse."

Nomenclature

$\dot{E}_v$ = monospectral power
F = monodirectional incident flux (monospectral)
I_v = monospectral intensity
q_{v_r} = monospectral hemispherically reflected flux
S = diffuse component shape factor
T = specular component shape factor
V_o = detecting system dark level
V_D = nonregularly reflected component
V_S = regularly reflected component
V_1 = nonregular reflection amplitude component
V_2 = regular reflection amplitude component
β = total scatter angle $= \psi + \theta$
δ = Dirac delta function
θ = angle of reflection
ν = frequency
ρ_v = monospectral reflectance function
$\bar{\rho}$ = residual
σ = rms roughness
ϕ = azimuthal angle (from the plane of incidence)
ψ = angle of incidence
ω = solid angle

Superscripts

$'$ = incidence variables
d = diffuse
s = specular

Subscripts

r = reflected
i = incidence

Introduction

AN empirical expression, which closely represents the radiant power reflected from surfaces, was developed and discussed by Look.[1,2] A parameter, referred to as a shape factor, S, was introduced in this empirical expression. If S equals 1, this expression can be reduced to the classical Lambert's reflection law. For a surface for which S is slightly greater than one, the shape factor corrected law has been shown to fit the actual data to within 2% and to within 7% for surfaces of engineering interest. In both of these cases, data were acquired by varying the angles of incidence and reflection such that their sum was constant. This was accomplished by rotating the surface. This procedure is slightly different than the one which is usually reported in the literature. That is, the angle of incidence is usually held constant while the angle of reflection is varied, i.e., the sum is not constant.

The present investigation extends the use of the aforementioned expression so that reflectance data representative of surfaces of engineering interest can be further analyzed. The reflectance data discussed herein were acquired by the "usual" procedure (i.e., different from that used by Look[2]), but the specimens are the same. The analytical effort has been concentrated on further establishing the mathematical expression introduced by Look.[2] This expression, which is a two-shape factor expression, consists of a near-diffuse component (nonregularly reflected), which can be described by the shape factor, S, and a near-specular component (regularly reflected), which can be described by the shape factor, T.

Instrumentation

The bidirectional flux measuring device shown schematically in Fig. 1 was used for the experiments in the present investigation. In the figure, the source, S, is a 54 w, tungsten ribbon filament, instrumentation lamp mounted in a light baffled enclosure. A folded optics configuration composed of a series of mirrors collects the radiant energy from the source, S, and refocuses this radiant energy with the spherical mirror, M_1, at T.

The scatter angle, β, is formed by the source and detector axes, and the plane formed by these axes is the plane of incidence. An orthogonal coordinate system can be constructed from the plane containing this angle. This coordinate system is fixed on the large rotatable arm which carries the source, source optics, and independently rotatable specimen mount. The first axis lies along the source optical axis in the direction of light propagation. The second axis of the system is normal to the plane and is situated at the apex of the angle, β. This second axis serves as

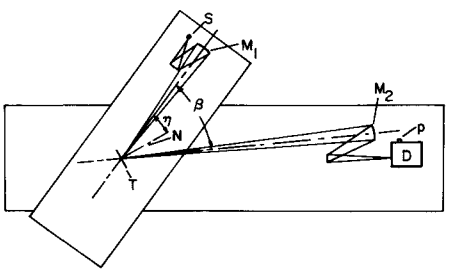

Fig. 1 Schematic of the experimental arrangement for the bidirectional reflectance measurements ($\eta = \psi$).

Received February 1, 1973, revision received December 7, 1973. Work supported under NSF Grant 5238. The author wishes to thank T. R. Sawheny for his efforts in the construction and calibration of the laboratory equipment, in data acquisition, and in helpful suggestions relative to experimental procedure.

Index categories: Thermal Surface Properties; Radiation and Radiative Heat Transfer.

* Associate Professor, Thermal Radiation Transfer Group, Department of Mechanical and Aerospace Engineering. Member AIAA.

the axis of rotation for the system. The third axis is in the β plane.

The orientation of the specimen surface is characterized by the angular position of its surface normal, N. The position is uniquely specified by the incidence angle, ψ, measured from the first axis of the system in the plane formed by the scatter angle, β. Notice that the scatter angle, β, is the sum of the angle of incidence, ψ, and the reflected angle, θ; $(\beta = \psi + \theta)$.

The radiant power scattered at an angle, β, is collected by the spherical mirror, M_2, and refocused at the aperture slit of a Perkin-Elmer Model 112 spectrometer, D. For the data presented, this instrument was adjusted so that only the radiant energy about 0.55 μ passed through to the detector. The mirrors, M_1 and M_2, are $4\frac{1}{4}$ in. in diameter and are first surface mirrors with a focal length of $21\frac{1}{2}$ in. An attached photomultiplier, P, is the detector. The response of this photomultiplier tube and measuring system was tested by using calibrated, neutral density, transmission filters. Within the precision of the measurements, the response was found to be linear over the range of experimental interest.

The voltage drop across the photomultiplier load resistors was measured as a function of β at preselected values of ψ. Voltage measurements were made by means of a multirange voltmeter, which has a calibrated accuracy and a departure from linearity of 1%/h.

Analysis

The monospectral intensity incident upon a flat surface is defined as

$$I_{\nu i} = \frac{dE_{\nu i}}{\cos\theta'\, dA'\, d\nu\, dt\, d\omega'} = \frac{d\dot{E}_{\nu i}}{\cos\theta'\, dA'\, d\omega'} \tag{1}$$

where $d\dot{E}_{\nu i}$ is the radiant monospectral power (per unit frequency), θ' is the angle of incidence, dA' is an increment of the illuminated area (Fig. 2), $d\nu$ is the frequency interval, and $d\omega'$ is the solid angle of the incident focused beam of radiant power. The primed variables represent the incident direction. Thus the increment of power per unit frequency incident upon the surface can be expressed as

$$d\dot{E}_{\nu i} = I_{\nu i} \cos\theta'\, d\omega'\, dA' \tag{2}$$

In an effort to model the experimental situation illustrated in Fig. 1 for the case of essentially monodirectional incidence in the direction (ψ_o, ϕ_o) or (μ_o, ϕ_o), the incident flux can be represented by the expression

$$F = I_{\nu i} \Delta\mu_o \Delta\phi_o \tag{3}$$

where μ_o equals $\cos\psi_o$, ψ_o represents the angles that describe the position of the incident beam with respect to the surface normal, ϕ_o is the azimuthal angle of the incident beam, and F is assumed constant.

In the case where the incident intensity is constant over a small solid angle of incidence from Eq. (3), the reflected intensity can be determined in general form without an explicit statement of the reflectance function. Thus

$$I_{\nu r} = (F/\pi)\rho_\nu(\mu, \phi, \mu_o, \phi_o)\mu_o \tag{4}$$

where $\rho_\nu(\mu, \phi, \mu_o, \phi_o)$ is referred to as a reflectance function.

To this point there has been no consideration of the surface; whether, it is "diffuse," "specular," or real. If the surface can be described as "diffuse," the reflectance function is defined as[3]

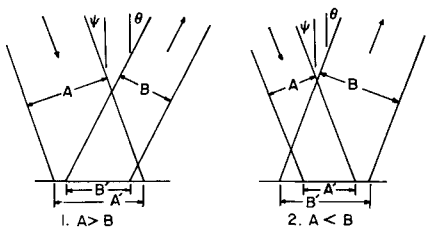

Fig. 2 Illustration of illumination-detection conditions.

$$\rho_\nu(\mu, \phi, \mu_o, \phi_o) = \rho_\nu \tag{5}$$

Thus, there is by definition no angular dependence, only frequency, and for the case where the surface can be described as "specular," the reflectance function can be defined as[3]

$$\rho_\nu(\mu, \phi, \mu_o, \phi_o) = (\pi/\mu)\rho_\nu(\mu, \phi)\delta(\mu_o - \mu)\delta[\phi_o - (\phi + \pi)] \tag{6}$$

The Dirac delta functions, denoted as $\delta[\phi_o - (\phi + \pi)]$ and $\delta(\mu_o - \mu)$, are discussed in detail by Love[3] and Born and Wolf.[4] Thus from Eq. (4), the reflected intensity can be obtained with the aid of Eq. (5) for the "diffuse" case. Therefore

$$I_{\nu r}(\text{Diffuse}) = F\mu_o \rho_\nu/\pi \tag{7}$$

In the case of the "specular" surface, Eq. (6) is substituted into Eq. (4) to obtain

$$I_{\nu r}(\text{Specular}) = F\rho_\nu(\mu, \phi)\delta(\mu_o - \mu)\delta[\phi_o - (\phi + \pi)] \tag{8}$$

The hemispherical flux reflected from the surface is defined as

$$q_{\nu_r} = \int_o^{2\pi} \int_o^{\pi/2} I_{\nu_r} \cos\theta\, d\omega \tag{9}$$

From an experimental point of view, one must be careful when using Eq. (9), which represents the received hemispherical flux, because the hemispherical flux is not received. That is, the field of view of the detecting optics system is essentially monodirectional. Therefore $I_{\nu_r} \cos\theta$ is assumed constant across this field of view of the detecting optics at an angle θ with respect to the surface normal and the remaining integral is represented by the receiving solid angle, $\Delta\omega$, in the "diffuse" case. Thus, by using the function of Eq. (7)

$$q_{\nu_r}{}^d = \int\int I_{\nu_r}(\text{Diffuse})\, \mu\, d\mu\, d\phi = \frac{F\mu_o \rho_\nu}{\pi} \cos\theta\, \Delta\omega \tag{10}$$

In the "specular" case, the delta functions of Eq. (8) dictate the form of the expression for the flux received. Thus, at the surface

$$q_{\nu_r}{}^s = \int\int I_{\nu_r}(\text{Specular})\, \mu\, d\mu\, d\phi = F\rho_\nu(\mu_o, \phi_o)\mu_o \tag{11}$$

The cases of experimental interest here are: 1) the area illuminated is larger than the area viewed (overilluminated), and 2) the area illuminated is less than the area viewed (overdetect). Figure 2 illustrates these situations.

The received monospectral power is defined as

$$\dot{E}_{\nu_r}(\theta, \phi) = \int\int q_{\nu_r}\, dB'$$

The following table presents the functional relationship for the above listed two cases in the "diffuse" and "specular" situations.

Table 1 Expected variation in the received monospectral power of pure diffuse and pure specular reflection

	$\dot{E}_{\nu_r}{}^d(\theta, \phi)$	$\dot{E}_{\nu_r}{}^s(\theta, \phi)$
Case I	$FB\rho_\nu\left(\frac{\Delta\omega}{\pi}\right)\cos\psi_o$	$FB\rho_\nu(\mu_o, \phi_o)$
Case II	$FA\rho_\nu\left(\frac{\Delta\omega}{\pi}\right)\cos\theta$	$FA\rho_\nu(\mu_o, \phi_o)$

Notice the relation $B = B'\mu_o$ was used for the "specular" cases and that $\dot{E}_{\nu_r}{}^s(\theta, \phi)$ is zero if $\phi \neq \phi_o$ and $\theta \neq \theta_o$.

Care must be taken to be cognizant of which case is involved when analyzing data. For example, for large angles of incidence and small-to-moderate angles of viewing, Case 1 is to be used; whereas, for large angles of viewing and small-to-moderate angles of illumination, Case 2 should be used. Note also that for some particular set of angles, ψ_m and θ_m, the area illuminated and viewed is equal $(A' = B')$. Thus

$$A/\cos\psi_m = B/\cos\theta_m \tag{12}$$

So for a "diffuse" surface, ψ assumed small and fixed, and $A > B$ (Case 1), the radiant power received will be constant as θ increases until $\theta = \theta_m$. From that angle on, the power received will decrease with $\cos\theta$ (Case 2). At the equal area point

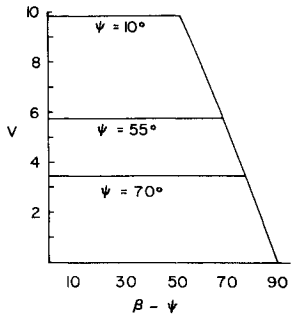

Fig. 3 Ideal variation in reflected power when the angle of incidence, ψ, is held fixed while the scatter angle, β, is varied.

$$\dot{E}_{v_r}{}^d = F\rho_v B\left(\frac{\Delta\omega}{\pi}\right)\cos\psi_m \qquad \text{(Case 1 variables)}$$

and

$$\dot{E}_{v_r}{}^d = F\rho_v A\left(\frac{\Delta\omega}{\pi}\right)\cos\theta_m \qquad \text{(Case 2 variables)}$$

Thus for a "diffuse" surface and ψ fixed, the output of the detecting system—the output voltage of the photomultiplier over its linear range—can vary as

$$\begin{aligned} V &= V_o + V_D\cos\psi = \text{const} \quad \text{for} \quad 0 \leqq \theta < \theta_m \\ &= V_o + V_D\left(\frac{A}{B}\right)\cos(\beta-\psi) \quad \text{for} \quad \theta_m \leqq \theta \leqq \frac{\pi}{2} \end{aligned} \qquad (13)$$

where $\beta = \psi + \theta$ and the dark level, V_o, and V_D, which is approximately proportional to $F(\Delta\omega/\pi)\rho B$, depends on the detector sensitivity. Figure 3 illustrates the variation indicated by Eqs. (12) and (13) if ψ is fixed.

Surfaces in general are not "diffuse" and in fact exhibit a certain degree of "specularity." In an attempt to account for this component and noting that this component appears to be symmetrical about the specular direction, if β is held constant,[2] an additional term was added to Eq. (13)

$$\begin{aligned} V &= V_o + V_D\cos\psi + V_s\cos\psi\cos(\beta-\psi), \quad \text{for} \quad 0 \leqq \theta < \theta_m \\ &= V_o + V_D\left(\frac{A}{B}\right)\cos(\beta-\psi) + V_s\cos\psi\cos(\beta-\psi), \\ &\qquad \text{for} \quad \theta_m \leqq \theta \leqq \frac{\pi}{2} \end{aligned} \qquad (14)$$

If one uses the empirical approach suggested by Look,[2] one must redefine

$$V_D = V_1\left[\frac{\cos\psi\cos(\beta-\psi)}{\cos^2\beta/2}\right]^{S-1}$$

and

$$V_S = V_2\left[\frac{\cos\psi\cos(\beta-\psi)}{\cos^2\beta/2}\right]^{T-1}$$

These definitions are made in order to allow the empirical formula to be as flexible as possible. In this representation, V_D represents the nonregularly reflected component, and when $S = 1$ reduces to the diffuse case (i.e., a constant), V_S represents the regularly reflected component and approaches a Kronecker delta function[5] at $\psi = \beta/2$ for T very large. By the very nature of these two components, T is always assumed to be larger than S. Thus, the received radiant power can be represented by

$$V = V_o + V_1 G^{S-1} g_1 + V_2 G^{T-1}\cos\psi\cos(\beta-\psi) \qquad (15)$$

where

$$\begin{aligned} G &= \cos\psi\cos(\beta-\psi)/\cos^2\beta/2 \\ g_1 &= \cos\psi \qquad\qquad \theta < \theta_m \\ &= (A/B)\cos(\beta-\psi) \qquad \theta \geqq \theta_m \end{aligned}$$

Equation (15) is based on the usual assumption that the two components of the received radiant power that are reflected are simply summable.

Specimen Characteristics

Two sets of specimen surfaces, (one set of 12 members, the other of 10) made of brass, were prepared for the experimental part of the investigation. All the specimens were cut to 1 in. square from $\frac{1}{4}$ in. thick stock. The initial step in the preparation procedure was to polish each surface to a high luster with a decreasing series of sizes of garnet paper. Next, each surface was lightly buffed with jeweler's rouge. Great care was taken not to overheat the surfaces during the buffing operation. If overheating occurred, the affected surface would exhibit a very slight scaly or orange-peel effect. An overheated surface was recycled until a mirrorlike appearance was observed with no visible surface blemish. Figure 4 is a highly magnified picture of a typical surface. The picture was taken with the aid of a scanning electron microprobe. It may be seen from this figure that, although not visible to the unaided eye, minute scratches did exist on the basic surface before the roughening procedure began.

The next step in the specimen preparation was to subject each surface to glass bead peening at various pressures. The machine used for this operation was supplied by the Zero Blast-N-Peen Div. of the Zero Manufacturing Co. With this machine, the first set (specimens 1–10, 16, 17) was peened with glass beads with a size range of 0.0555 to 0.0661 in. in diameter. A hand-held spacer was used to position each specimen exactly 6 in.

Fig. 4 Typical polished brass surface before peening with glass beads (surface character magnified × 1000).

Table 2 Pressures used in peening brass surfaces, description of coverage procedures and surface roughness estimates

Specimen no.	Pressure, psig	Coverage[a]	rms (μ-in.)	AA (μ-in.)
1	15	v.l.	20	20
2	15	h.	65	50
3	20	v.l.	35	30
4	20	h.	70	65
5	30	v.l.	40	35
6	30	h.	95	80
7	40	v.l.	60	50
8	40	h.	105	90
9	50	v.l.	60	50
10	50	h.	110	100
16	70	m.	80	80
17	90	m.	120	100
20	40	v.h.	50	40
21	40	h.	16	15
22	40	l.	12	11
23	40	v.v.l.	5	4
24	80	v.h.	45	43
25	80	h.	30	28
26	80	l.	13	11
27	80	v.l.	5	3.5
28	100	h.	47	45
29	···	mirror	1.8	1.8

[a] v.l. = very lightly; v.v.l. = very, very lightly; h. = heavily; v.h. = very heavily; m. = moderately.

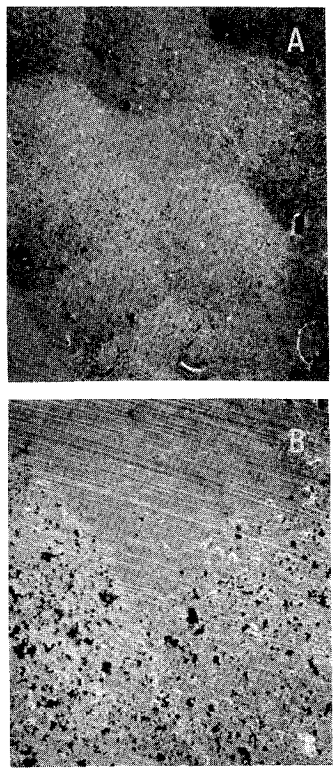

Fig. 5 Brass surface heavily peened at 20 psig with glass beads of average diameter of 0.061 in. a) ×100; b) ×300.

from the muzzle of the peening gun. The second set of specimens (20–29) was peened with glass beads with a size range of 0.0017 to 0.0035 in. in diam. The glass beads used were manufactured from a high grade optical crown glass, essentially free of lead, and were spherical in shape. Table 2 is a list of the various pressures used and surface coverage descriptions of the roughened surfaces of the specimens. An estimate of roughness of each specimen, as indicated by a Bendix profilometer, is included in the table. Both numbers are measured in micro-inches (μ-in.) and are supposed to represent root-mean-square (rms) and arithmetic average (AA) values.

Figure 5 illustrates the effect of the glass sphere impact. This figure depicts the surface of Specimen 4. Notice in addition to the spherical cap-like dent that a large number of very small cavities (the little black specks) appear within it. This condition was caused by glass beads whose surfaces were rough. The small cavities were produced upon impact of these beads.

Data Acquisition Procedure

Data were obtained for various values of the angle of incidence, ψ. The actual procedure of data acquisition was to use changes in the scatter angle, β, in the cases of ψ equal to 10°, 30°, 50°, 70°, or

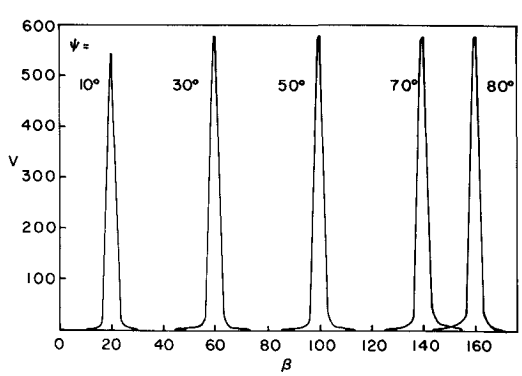

Fig. 6 Raw data from Specimen 23 of reflected power vs scatter angle, β.

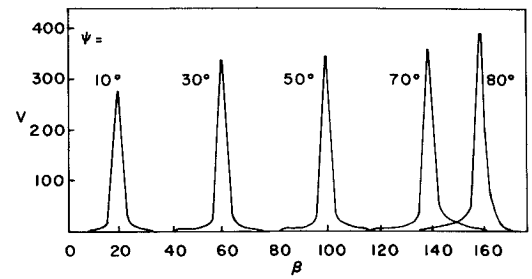

Fig. 7 Raw data from Specimen 22 of reflected power vs scatter angle, β.

80°. Thus, β (which equals $\psi+\theta$) is the independent variable. The scatter angle, β, was allowed to vary from 8° to $\psi+90°$ in such a way that the increase or decrease in voltage from the preceding reading did not exceed approximately three percent of the peak value. The only exceptions to this were the mirror-like surfaces, e.g., Specimen 29, where the increase in voltage with angle was extremely high.

Data Reduction Procedure

The reduction of the data, based on the use of Eq. (15) was accomplished by means of a least squares iterative procedure. This procedure was programmed for an IBM 360/50 digital computer. In the procedure, the method of least squares was used to calculate the dark level, V_o, the nonregular reflection amplitude component, V_1, and the regular reflection amplitude component, V_2. These factors correspond to the initially assumed values of the nonregularly reflecting shape factor, S, and the regularly reflecting shape factor, T. Another least squares procedure was then used to correct S and T and so on. A residual, $\bar{\rho}_i(\beta)$, was determined for each data pair, and the variance, VAR, was calculated for each set of data values. These quantities are defined as follows:

$$\bar{\rho}_i \doteq V_i - V_o - V_1 G^{S-1} g_1 - V_2 G^{T-1} \cos\psi \cos(\beta-\psi) \quad (16)$$

$$\mathrm{VAR} = \frac{\sum_{i=1}^{N} \bar{\rho}_i^{\,2}}{N} - \left(\frac{\sum_{i=1}^{N} \bar{\rho}_i}{N}\right)^2 \quad (17)$$

For data which exhibited the so-called off-specular peak, an artificial incidence angle was determined and introduced to force a fit of Eq. (15) to the data. The minimum of the variance corresponds to the most probable fit of the expression given by Eq. (15) to the experimental data.

Data Analysis Results

Figures 6–9 illustrate the bidirectionally reflected received power of only four of the specimens. These were selected as

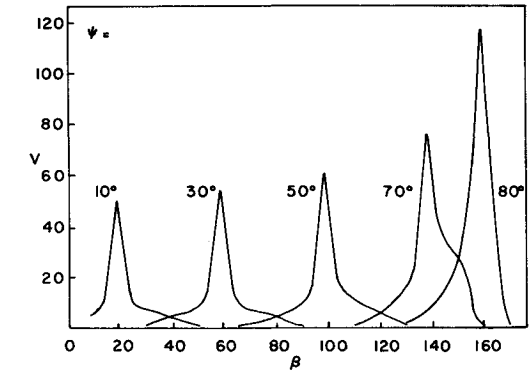

Fig. 8 Raw data from Specimen 21 of reflected power vs scatter angle, β.

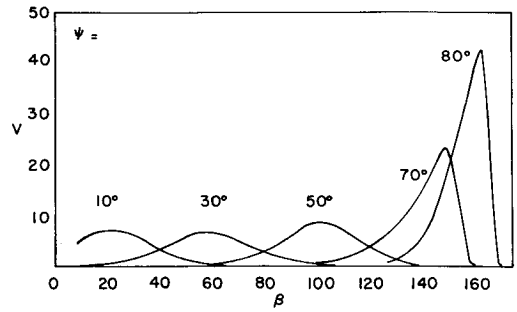

Fig. 9 Raw data from Specimen 20 of reflected power vs scatter angle, β.

being typical of all the data taken. Graphically, the pictures indicate that continued peening greatly reduces the regularly reflected component, while broadening the nonregularly reflected component. Specimen 23 (Fig. 6) exhibits very strong glare, whereas, Specimen 20 (Fig. 9) can be generally described as more "diffuse." In Fig. 8, the data presented for the case of $\psi = 70°$ appear to have an unusual shape. This phenomenon may be the conductor analog to the angular distribution of radiation reflected from roughened dielectric surfaces reported by Smith et al.[6] At the present time, this characteristic is being investigated.

After the least squares data reduction, it was found that the statistically determined nonregular component parameters, S and V_1, followed no definite variation with ψ when the specimen exhibited very strong glare characteristics (e.g., Specimen 23); while the regular components did. In fact, in the majority of these cases, V_1 was essentially zero. Similarly, for models whose characteristics were similar to Specimen 20, parameters T and V_2 followed no definite variation with ψ while the nonregular components did. For the "in-between" surfaces, whose characteristics were similar to Specimens 21 and 22, all components followed definite variations with ψ. As for the aforementioned variations, V_1 and V_2 increased with ψ (in a fashion similar to that discussed by Look[1]), while the variations in S and T were essentially proportional to $\cos^2\psi$. Figures 10 and 11 depict the residuals, defined by Eq. (20) for Specimens 20 and 23. It can be easily seen that the fit of Eq. (15) to these data is quite good (being better for the nonregularly reflecting models). These two examples are typical and are presented because they represent the two extremes in the reflection characteristics encountered.

Finally, it was determined that S decreased with roughness, while T was essentially independent of the roughness. In fact, it was observed that the rms roughness and the nonregular shape factor, S, approximately followed the expression

$$S\sigma = \text{const} \tag{18}$$

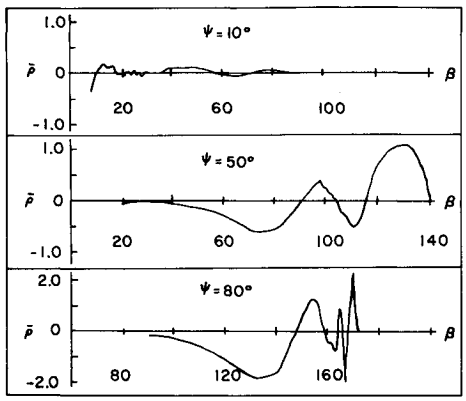

Fig. 10 Typical data of the residual, $\bar{\rho}$, vs scatter angle, β, for Specimen 20. a) $\psi = 10$, V (peak value) = 7.1, b) $\psi = 50$, V (peak value) = 8.6, c) $\psi = 80$, V (peak value) = 41.9.

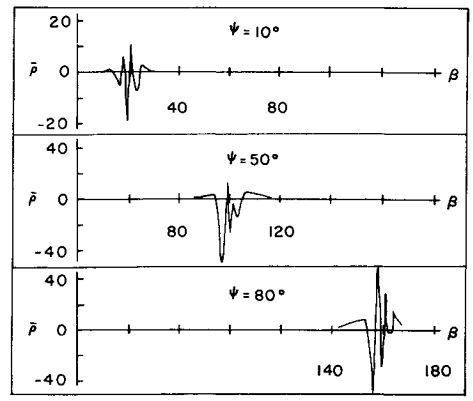

Fig. 11 Typical data of the residual, $\bar{\rho}$, vs scatter angle, β, for Specimen 23. a) $\psi = 10$, V (peak value) = 540, b) $\psi = 50$, V (peak value) = 577, c) $\psi = 80$, V (peak value) = 577.

Summary

The bidirectionally reflected power from a number of flat metal surfaces of engineering interest was investigated. An empirical expression, introduced by Look[1] and later modified by Look,[2] was found to represent the reflected radiant power from these surfaces when a completely different data acquisition technique was used than was applied earlier by Look.[1,2] Though these surfaces exhibited very diverse reflection characteristics, the empirical expression fit the data quite well.

In addition, the trends in the variation of the parameters of the empirical expression were consistent regardless of the data acquisition procedure. That is, in Look's work,[2] S and T were strong functions of $\beta/2$. This angle is equivalent to the angle of incidence, ψ, in this report. The statistically determined amplitude functions, V_1 and V_2, also exhibited the same characteristics regardless of the data acquisition technique.

Measurement of in-surface parameters yielded information concerning the relation between both the nonregular and regular shape factors and the surface roughness, σ. Of particular interest was the fact that not only did S decrease as σ increased (for the more nonregularly reflecting surfaces) and T was essentially independent of σ (for the more regularly reflecting surfaces) but that the same characteristic relationships were determined independent of the data acquisition technique.

Off-specular peaks were encountered in this investigation (e.g., Fig. 9). Equation (15) was easily manipulated to this into account.

Thus, it appears that the hypotheses underlying the development of Eq. (15) were adequate, and this equation can be used to represent the radiant power reflected from surfaces. Further the magnitudes and variations of the statistically determined parameters with ψ (or β) may be useful in classifying surfaces.

References

[1] Look, D. C., "Diffuse Reflection from a Plane Surface," *Journal of the Optical Society of America*, Vol. 55, No. 12, Dec. 1965, pp. 1628–1632.

[2] Look, D. C., "Angular Distribution of Radiation Reflected from Roughened Brass: Experiment and Analysis," AIAA Paper 73-151, Washington, D.C., 1973.

[3] Love, T. J., *Radiative Heat Transfer*, C. E. Merrill Publishing Co., Columbus, Ohio, 1968, p. 42.

[4] Born, M. and Wolf, E., *Principles of Optics*, Pergamon Press, New York, 1970, p. 755.

[5] Mathews, J. and Walker, R. L., *Mathematical Methods of Physics*, W. A. Benjamin, Inc., New York, 1964, p. 96.

[6] Smith, A. M., Müller, P. R., Frost, W., and Hsia, H. M., "Super- and Subspecular Maxima in the Angular Distribution of Polarized Radiation Reflected from Roughened Dielectric Surfaces," *AIAA Progress in Astronautics and Aeronautics: Vol. 24, Heat Transfer and Spacecraft Thermal Control*, edited by J. W. Lucas, MIT Press, Cambridge, Mass., 1970, pp. 249–269.